Remote Sensing Applications: Society and Environment 26 (2022) 100760

Contents lists available at ScienceDirect

Remote Sensing Applications: Society and Environment

journal homepage: www.elsevier.com/locate/rsase

Assessment of drought time-frequency relationships with local atmospheric-land conditions and large-scale climatic factors in a tropical Andean basin

Alexandra Nieves [a], Juan Contreras [a,c], Jheimy Pacheco [c], Javier Urgilés [a], Fernado García [a,b], Alex Avilés [a,b,*]

[a] Carrera de Ingeniería Ambiental, Facultad de Ciencias Químicas, Universidad de Cuenca, Eco Campus Balzay, Av. Victor Albornoz y Calle de los Cerezos, Cuenca, 01.01.168, Ecuador

[b] Grupo de Evaluación de riesgos ambientales en sistemas de producción y servicios (RISKEN), Universidad de Cuenca, Eco Campus Balzay, Av. Victor Albornoz y Calle de los Cerezos, Cuenca, 01.01.168, Ecuador

[c] Instituto de Estudios de Régimen Seccional del Ecuador (IERSE), Universidad del Azuay, Av. 24 de mayo 7-77 y Hernán Malo, Cuenca, 010204, Ecuador

ARTICLE INFO

Keywords:
Drought indices
Vegetation
Local atmospheric conditions
Macroclimatic indices
Wavelet coherence
Tropical andean basin

ABSTRACT

This study analyzed in the Tomebamba subbasin the relationships between droughts, the condition of the vegetation, global scale climatic indices and local atmospheric variables. The variability of monthly meteorological and hydrological droughts, as well as the condition of the vegetation, were characterized using the standardized precipitation index (SPI), the standardized streamflow index (SSI), and the vegetation condition index (VCI). The wavelet coherence method was used to establish time-frequency relationships. The results indicate that the vegetation in good condition reduces the impact of hydrological drought events when there are no sudden precipitation impacts. The atmospheric variables at the local scale with the highest significant correlation are cloud cover, relative humidity, specific humidity, temperature and specific rainwater content between 500 and 750 hPa. The Multivariate ENSO Index (MEI), ENSO 3, the Southern Oscillation Index (SOI), the Pacific Decadal Oscillation (PDO), and the Pacific North American Index (PNA) are strongly linked to SPI and the ENSO 4 index to SSI. Vegetation does not show strong relationships with any climate indices, obtaining the best relationship with the PNA. The results provide a basis for the analysis of variability and propagation of the droughts in Andean basins, their relationships with local and large-scale factors, and the influence of drought on vegetation.

1. Introduction

Drought is a natural non-permanent phenomenon and recurring water scarcity (Dracup et al., 1980; Hao and Singh, 2015; Mishra and Singh, 2010) and one of the most expensive climate-related hazards around the world (Wardlow et al., 2012; Wilhite, 2000; Zhong et al., 2021), causing societal problems, economic losses and ecological system detriment (Choat et al., 2012; Crausbay et al., 2017; Kogan et al., 2013; Piao et al., 2010; UNESCO, 2020). From 1995 to 2015, droughts represented 5% of natural disasters, harming 1.1

* Corresponding author. Universidad de Cuenca, Av. 12 de abril s/n y Loja, Cuenca, 010203, Ecuador.
E-mail address: alex.aviles@ucuenca.edu.ec (A. Avilés).

https://doi.org/10.1016/j.rsase.2022.100760
Received 24 April 2021; Received in revised form 12 April 2022; Accepted 15 April 2022
Available online 20 April 2022

billion people and causing U.S. $100 billion in economic losses (UNESCO, 2020). Unlike other natural hazards, drought is recognized as a complex and multifaceted phenomenon that occurs both in high and low rainfall areas (Van Loon et al., 2016b; Wang et al., 2020; Wilhite and Glantz, 1985). Therefore, for a better understanding and study of droughts, it has been classified into a meteorological, hydrological, agricultural, and socio-economic drought (Wilhite and Glantz, 1985).

Meteorological drought is related to a period with abnormally low precipitation (Mishra and Singh, 2010). Hydrological drought follows meteorological drought causing a scarcity in surface, and subsurface water (Van Loon, 2015), this type of drought can be modified simultaneously by reservoirs or landscape conditions (Van Loon and Laaha, 2015; Wu et al., 2016). Moreover, natural processes such as photosynthesis, evaporation, and transpiration of vegetation play an essential role in the hydrological cycle by directly and indirectly affecting the basin water fluxes (Alvarenga et al., 2016; Carlson and Arthur, 2000). Scarce precipitation, decreased soil moisture and streamflow or any combination of three trigger agricultural drought, which immediately impacts crop production and vegetation condition (Dracup et al., 1980; Mishra and Singh, 2010). As a consequence of unsatisfied water demand, adverse effects on irrigation, streamflow and vegetation, the socio-economic drought arises (Guo et al., 2019). Socio-economic drought is a non-physical phenomenon associated with local water supply, which leads to water demand problems through socioeconomic systems (Tu et al., 2018).

Meteorological and vegetation indices based on ground and remote sensing information have been widely used to monitor droughts. Since Standardized Precipitation Index (SPI) (McKee et al., 1993) and Standardized Streamflow Index (SSI) (Vicente-Serrano et al., 2012) are solely based on precipitation and streamflow, respectively, both indices are frequently used to characterize the change of meteorological to hydrological droughts (Real-Rangel et al., 2020; Wu et al., 2017; Yu et al., 2020). Meanwhile, for agricultural drought detection have been applied indices such as Crop Moisture Index (CMI) (Palmer, 1968), Normalized Difference Vegetation Index (NDVI), Vegetation Condition Index (VCI) (Kogan, 1995), Vegetation Health Index (VHI) (Kogan, 1997), Vegetation drought index (VDI) (Sun et al., 2013), Spectral vegetation index (SVI) (Sun et al., 2017), Scaled Drought Condition Index (SDCI) (Rhee et al., 2010), Normalized Difference Latent Heat Index (NDLI) (Liou et al., 2019)(Liou et al., 2019) among others. This last approach derived from remote sensing represents the latent heat on the earth's surface and, therefore, the dynamics of the states of water in the hydrological cycle. However, other studies condider that NDVI, VCI, and VHI are suitable indices from remotely sensed data to study the response of vegetation to drought (Aquino et al., 2021; Casa et al., 2021; Dalezios et al., 2000; Dutta et al., 2015; Khosravi et al., 2017; Zambrano et al., 2016).

Drought propagation refers to the analysis response of one type of drought to another (Huang et al., 2015; Wu et al., 2017). The study of drought propagation is essential to understand complex relationships among different types of drought (Hao and Singh, 2015). Relationships between droughts are often linked to natural factors such as climate (Cerón et al., 2020; Ganguli and Janga Reddy, 2013; Madadgar et al., 2016; Mulualem and Liou, 2020; Shahid, 2008; Tadesse et al., 2004; Wang et al., 2019), human activities or a combination of two (Baek et al., 2017; Berghuijs et al., 2014; Tijdeman et al., 2018; Van Loon et al., 2016b). Hence, several studies revealed that climate variables such as El Niño–Southern Oscillation (ENSO) and Pacific Decadal Oscillation (PDO) could aggravate the characteristics, duration, and intensity of droughts (Mortensen et al., 2018; Oliveira-Júnior et al., 2018; Vicente-Serrano et al., 2011, 2017). Other studies have analyzed the relationship between drought types in wet and dry tropical areas considering the effect of atmospheric and land variables (Imfeld et al., 2019; Marengo and Espinoza, 2016; Mortensen et al., 2018; Real-Rangel et al., 2020; Tramblay and Hertig, 2017; Vicente-Serrano et al., 2017; Zambrano Mera et al., 2018) simultaneously. In addition, studies have shown

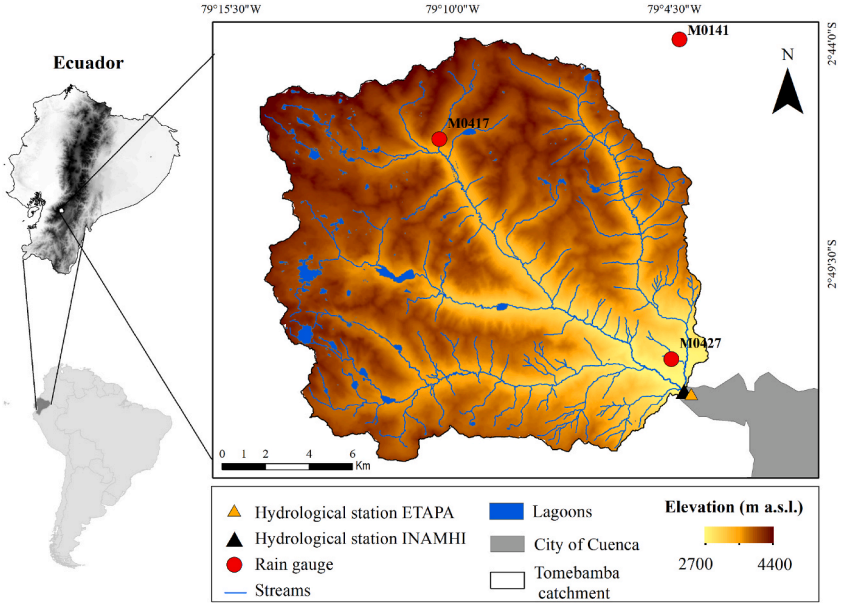

Fig. 1. The Tomebamba subbasin and location of the meteorological stations.

the complex interplay among precipitation patterns, streamflow, vegetation, soil moisture and atmosphere phenomenon cause different catchments around the world to have a different response to drought (Ding et al., 2021; Gebrehiwot et al., 2011; Gómez-Limón, 2020; Javed et al., 2020; Jiang et al., 2022; Rousta et al., 2020; Wang et al., 2016; Wu et al., 2016; Zhang et al., 2015).

Many investigations have focused on tropical Andes catchments due to the hydrological importance and various ecosystem services (Bonnesoeur et al., 2019; Buytaert et al., 2006; Célleri and Feyen, 2009; Cincotta et al., 2000; Flores-López et al., 2016; Ochoa-Tocachi et al., 2016). Even though studies have been carried out specifically on droughts in Andean ecosystems (Avilés et al., 2015, 2016; Campozano et al., 2020a; Valverde-Arias et al., 2018; Zambrano Mera et al., 2018; Zhiña et al., 2019), there is still a lack of knowledge about the relationships between droughts and its relations with hydrometeorological and climatic conditions. Therefore, the study aims to perform a drought time-frequency analysis with local atmospheric-land conditions and large-scale climatic factors in a tropical Andean catchment of southern Ecuador. The main objectives we seek to address were: 1) to characterize droughts using SPI, SSI and VCI indices, 2) establish relationships between drought indices and 3) define the relationship among drought indices and atmospheric-land variables and large-scale climatic indices. This study presents the first exploration of relationships among meteorological, hydrological and agricultural droughts (referring to the condition of vegetation) in a tropical Andean basin. This study also provides valuable insights about local/regional and global atmospheric drivers that control droughts in the study area and the region.

2. Methods and materials

2.1. Study area

The investigation was conducted in the upper and middle part of the Tomebamba river subbasin, located in the Southern Ecuadorian Andes. This basin is located in the inter-Andean depression, covering the latitude 2°43' – 2°54′S and longitude 79°15' – 79° 3′W (Fig. 1). Its elevation varies between 2700 and 4400 m above sea level (m a.s.l.) and covers an area of approximately 300 km^2. The climate of the catchment is influenced by the continental air masses of the Amazon basin, by the seasonal change of the Intertropical Convergence Zone, and by the Humboldt ocean current, resulting in the formation of convective and orographic clouds (Bendix et al., 2006). Predominant soil types are Andosols and Histosols (Muñoz et al., 2018). The upper part of the basin (>3500 m a.s.l.) is a natural area covered by a mix of wetlands, lagoons, and páramo grasslands. The middle land landscapes (2700–3500 m a.s.l.) are composed of a mosaic of forest, agricultural/grazing, and sparse urban settlements. Approximately 40% of the basin area belongs to the Cajas National Park. The Tomebamba subbasin provides drinking water, water for irrigation and industry for Cuenca, the third-largest city in Ecuador with nearly 580000 inhabitants (Muñoz et al., 2018).

2.2. Data series

The monthly precipitation for the period 1976–2014 (38 years) of three weather stations (see Table 1) of the National Institute of Meteorology and Hydrology of Ecuador (INAMHI) were used for the characterization of the meteorological droughts. Data gaps in the rainfall time series were filled using the MissForest imputation method (Stekhoven and Bühlmann, 2012). The monthly average rainfall of the study area was obtained through the Thiessen polygons method (Brassel, 1979). INAMHI also provided the monthly streamflow data of the Matadero en Sayausi gauge station (outlet of the upper and middle part of the Tomebamba subbasin) for 1968–2014 (46 years). Streamflow series contained around 5% gaps, which were filled through linear regression ($R^2 = 0.91$) using data from the ETAPA EP station, Cuenca's drinking water enterprise, located few meters downstream of the Matadero en Sayausi gauge station (Fig. 1). The filled streamflow series were used for the hydrological drought characterization.

EVI satellite images from the Terra Moderate Resolution Imaging Spectroradiometer (MODIS) Vegetation Indices (MOD13Q1) Version 6 data, generated every 16 days at 250 m spatial resolution as a Level 3 product, were downloaded for the period 2000–2014 (Dutta et al., 2015). The downloading procedure was carried out using the Application for Extracting and Exploring Analysis Ready Samples (AppEEARS) developed by the United States Geological Survey (USGS, https://lpdaac.usgs.gov/product_search/). In addition, the datasets were downloaded of following synoptic-scale climate indices: Bivariate ENSO Time Series (BEST) (Smith and Sardeshmukh, 2000), Multivariate ENSO Index (MEI) (Wolter and Timlin, 2011), North Atlantic Oscillation Index (NAO) (Barnston and Livezey, 1987), ENSO 1 + 2, ENSO 3, ENSO 4, ENSO 3.4 (Trenberth, 2016), Oceanic Niño Index (ONI) (Yu et al., 2011), Pacific Decadal Oscillation (PDO) (Mantua and Hare, 2002), Pacific North American Index (PNA) (Ebdon, 1960), Quasi-Biennial Oscillation (QBO) (Reed et al., 1961), Southern Oscillation Index (SOI) (Troup, 1965), Tropical Northern Atlantic Index (TNA) (Enfield et al., 1999), Trans-Niño Index (TNI) (Trenberth and Stepaniak, 2001), and the Tropical Southern Atlantic Index (TSA) (Rajagopalan et al., 1998). The time series are available at https://www.esrl.noaa.gov/psd/data/climateindices/list/. These indices were chosen in analogy with various studies in the Andean Region in which the selected Tomebamba subbasin is located (Ballari et al., 2020; Campozano et al., 2016, 2018; Esquivel-Hernández et al., 2019; Mendoza et al., 2019; Mora and Willems, 2012; Tobar and Wyseure, 2018; Vuille et al.,

Table 1
Hydrological and rain gauge stations considered in the study.

Code	Name	Longitude	Latitude	Elevation (m a.s.l.)	Mean annual rainfall/streamflow	Missing values (%)
M0141	El Labrado	79°04′23″ W	2°43′54″ S	3335	1268[a]	11.1
M0417	Piscicola Chirimachay	79°10′20″ W	2°46′24″ S	3270	1280[a]	13.2
M0427	Sayausi (Matadero DJ.)	79°04′34″ W	2°51′53″ S	2780	1037[a]	3.2
H0896	Matadero en Sayausí	79°04′23″ W	2°52′32″ S	2693	7.0[b]	5.5

[a] Unit in mm.
[b] Units in m^3/s.

2000).

Monthly averaged reanalysis data from the European Center for Medium-Range Weather Forecasts Re-Analysis version 5 (ERA-5) were downloaded for the study area. ERA-5 has a horizontal resolution of 0.25° × 0.25° and a temporal coverage from 1979 to the present. Several estudies have demonstrated the superiority of ERA-5 estimates in hydrological evaluations over other reanalysis products such as ERA-Interim (Tarek et al., 2020), Climate Forecast System Reanalysis, Modern Era Retrospective Analysis for Research and Applications version 2, and the Japanese 55-a-Reanalysis project (Mahto and Mishra, 2019). For our study, seven atmospheric variables at local scale were considered, including the fraction of cloud cover, geopotential, relative humidity, specific cloud liquid water content, specific humidity, specific rainwater content and temperature. All these variables were downloaded for 14 pressure levels (from 200 to 850 hPa - in intervals of 50 hPa) for the period 1979–2014. The reanalysis data was downloaded from the Copernicus repository (https://cds.climate.copernicus.eu).

2.3. Methods

SPI determines the deficit or excess of precipitation in a given location and period. This index was calculated on a monthly scale (SPI1) following the methodology proposed by McKee et al. (1993). Data were adjusted to a gamma probability distribution which subsequently was transformed into a standardized normal distribution. According to McKee et al. (1993), the classification of wet and dry events is shown in Table 2.

The Standardized Streamflow Index (SSI), used to characterize hydrological droughts, was calculated on a monthly scale (SSI1) following the methodology proposed by Vicente-Serrano et al. (2012). For this, the streamflow data were filtered by months (January to December), obtaining 12 series adjusted to different probability distributions: Chi-square, Gamma, Logistics, Log-normal, and Normal and Weibull (Penalba and Rivera, 2016; Vicente-Serrano et al., 2012). The theoretical distribution that best represented the behavior of the analyzed streamflow data was determined using the Anderson-Darling (A.D.) goodness of fit statistical test (Penalba and Rivera, 2016). The selected probability distribution was transformed into a normal distribution to derive the SSI, of which the values were classified according to the classification proposed by Vicente-Serrano et al. (2012) (Table 3).

Generally, the elements of drought characterization include the duration, magnitude and severity of the drought event (Thomas et al., 2014). The thresholds for the quantification of those variables were selected from Fleig et al. (2006), Tallaksen and Van Lanen (2004), and Van Loon et al. (2016a). The *duration of a drought event* corresponds to the number of consecutive months with an SPI or SSI value below the threshold (−1, corresponding to moderate drought). The *magnitude* is equal to the sum of the deficit from the threshold during a drought event, and for *severity,* two types were considered. The first, called maximum severity, is defined by the maximum deviation regarding the threshold and the second, the average severity, represents the division between the magnitude and duration of a dry event.

The vegetation state was calculated with the Vegetation Condition Index (VCI) using values of EVI as input (see Eq. (1)). $VCI_{i,j,k}$ is the index value within pixel *i*, during the analysis period *j* (every 16 days according to MODIS sensor), for the year *k*; $EVI_{i,j,k}$ is the EVI index value for pixel *i*, for the period *j* and the year *k*; $EVI_{i;min}$ and $EVI_{i;max}$ correspond to the minimum and maximum value of the EVI index evaluated over several years (or the total period of analysis), for pixel *i*.

$$VCI_{i,j,k} = \frac{EVI_{i,j,k} - EVI_{i;min}}{EVI_{i;max} - EVI_{i;min}} * 100 \quad (1)$$

The spatially averaged VCI values on a monthly scale (VCI1) were classified using the ranges presented by Kogan (1995). Vegetation is considered in good condition in 40–100%; lower values represent vegetation stress, and the closer to 0%, the worse the vegetation state.

The Wavelet Coherence method (W.C.) was used to analyze the relationships between SPI1, SSI1 and VCI1 and their relationships with global climate indices and local-scale atmospheric variables. The method was applied with a significance level of 5%. The basic principle of the Continuous Wavelet Transform (CWT) is to derive coefficients, a function of frequency and time and measures the similarity between a signal and an analysis function. In this case, the signal corresponds to the time series, and the function is a prototype wavelet (mother wavelet). Different wavelet families have been developed according to the purpose of the analysis. Daubechies, Haar, Symlets, and Coiflets families are often used for discrete transforms. On the other hand, Gauss, Morlet and Mexican hat are used for continuous transforms. Commonly for studies of geophysical time series, the Morlet family is used, which allows better extraction of the characteristics of a signal by providing a good balance between time and frequency location. The Morlet wavelet is defined according to equation (2) (Grinsted et al., 2004), where ω_0 is a dimensionless frequency, and η is the time multiplied by a scale factor.

Table 2
Classification of meteorological drought according to SPI.

Category	SPI Value
Extreme Drought	(-∞, −2]
Severe Drought	(-2, −1.5]
Moderate Drought	(-1.5, −1]
Normal	(-1, 1)
Moderately humid	[1, 1.5]
Very wet	[1.5, 2)
Extremely wet	[2, ∞)

Table 3
Classification of hydrological drought according to SSI.

Category	SSI Value
Extreme Drought	(-∞, −2)
Severe Drought	[-2, −1.5)
Moderate Drought	[-1.5, −1)
Mild drought	[-1, 0)
Normal	[0, +∞)

$$\psi_0(\eta) = \pi^{-\frac{1}{4}} e^{i\omega_0\eta} e^{-\frac{1}{2}\eta^2} \tag{2}$$

The continuous transform of x_n, with x_n a time series with equal intervals δ t and localized time index n = 0 … N-1 (Torrence and Compo, 1998), is defined as the convolution of x_n with a scaled and displaced version of $\psi_0(\eta)$, as shown in equation (3), where, δ t is the analysis time interval, s the scale, x_n the time series, and ψ_0 the determined mother wavelet (Grinsted et al., 2004).

$$W_n^X(s) = \sqrt{\frac{\delta t}{s}} \sum_{n=1}^{N} x_n \psi_0 \left[(n' - n)\frac{\delta s}{s}\right] \tag{3}$$

Finally, the wavelet power can be defined as $|W_n^X(s)|^2$ which is used to represent the energy contained in the time series. Due to the finite length of time series are the errors located at the beginning and end of the transform, and to handle the errors, a cone of influence (COI) is introduced. Results located outside or near the limits of the cone should be treated carefully because of the edge effects. Such effects become essential in this region, being necessary to analyze whether the obtained data are the product of chance or a true change in the variance of the series (causality) (Torrence and Compo, 1998).

The statistical significance of the wavelet power was calculated using the method proposed by Torrence and Compo (1998), which consists of generating a random background signal and comparing it with the wavelet power. The null hypothesis is that the time-series signal is generated by a stationary process with a background power signal. A 5% significant level is used for this method, which is equivalent to a 95% confidence level. If needed to analyze the similarity between two wavelet signals derived from two different time series, it is inaccurate only to compare the wavelet power of each one separately. That is why procedures such as Crossed Wavelet Transform have been developed and from this the Wavelet Coherence. Cross Wavelet Transformed identifies common areas with high energy between the series. Its primary principle states: Assuming that $W_n^X(s)$ and $W_n^Y(s)$, are continuous wavelets transforms of two time series: $X = \{x1, x2, \ldots, xn\}$ y $Y = \{y1, y2, \ldots, yn\}$, the Cross Wavelet Transform between them would be $W_n^{XY}(s) = W_n^X(s) W_n^{Y^*}(s)$, where $W_n^{Y^*}(s)$ represents the conjugate complex of $W_n^Y(s)$ and s is the scale (Lin et al., 2017).

Finally, the Wavelet Coherence measures the covariance between X and Y series in the time-frequency plane, using the Cross Wavelet Transform as the basis. Wavelet Coherence is calculated according to equation (4), where R^2 represents the quadratic coherence or coherence level (the closer to 1, the higher correlation), S is a smoothing operator that depends on the wavelet family used, and $W_n^{XY}(s)$ is the Cross Wavelet Transform (Grinsted et al., 2004).

$$R_n^2(s) = \frac{\left|S\left(s^{-1} W_n^{XY}(s)\right)\right|^2}{S\left(s^{-1}\left|W_n^X(s)\right|^2\right) \cdot S\left(s^{-1}\left|W_n^Y(s)\right|^2\right)} \tag{4}$$

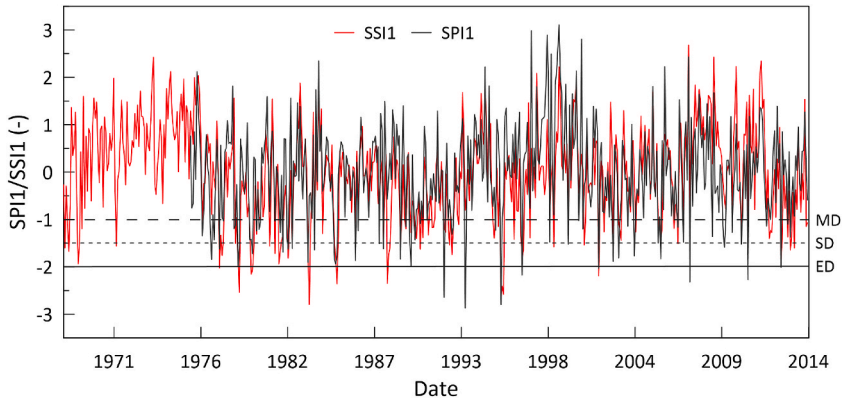

Fig. 2. Times series of monthly meteorological (SPI1) and hydrological (SSI1) droughts. MD: Moderate Drought, SD: Severe Drought, ED: Extreme Drought.

3. Results and discussion

3.1. Evolution and frequency of the meteorological droughts

The time evolution of SPI1 for 1976–2014 is depicted in Fig. 2. Droughts with highest severities correspond to −2.86 (May/1993), −2.79 (Aug/1995) and −2,64 (Jan/1992). The duration of most identified drought events is 1-month, and the longest drought event lasted 3-months and occurred in the period Oct/1979–Dec/1979, Feb/1985–Apr/1985 and Ago/2009–Oct/2009. Fig. 3 shows the monthly frequency analysis of the extreme, severe and moderate meteorological droughts. It is observed from the figure that moderate drought events score the highest frequency followed by severe and extreme events. Based on the SPI1 values for the period 1980–2010, some of the identified events are similar to the events in the region published by Pacheco et al. (2017). These authors found that the driest months were May and November in 1985, July 1990, August 1992, and June and September 2002.

3.2. Evolution and frequency of the hydrological droughts

The time evolution of the SSI1 is shown in Fig. 2. The driest periods correspond to Nov/1977–Feb/1978, Oct/1979–Jan/1980, Aug/1981–Nov/1981, Feb/1985–May/1985, Jun/1988–Aug/1988 and Aug/1985–Oct/1985. The most recurrent dry month was February. However, the month with the highest average severities was July. The frequency distribution of extreme, severe and moderate hydrological drought events are depicted in Fig. 3, illustrating that moderate drought events prevail over the two other drought categories. Furthermore, it was observed that the total percentage of dry months did not exceed 20% of all analyzed months.

3.3. Characterization of the vegetation condition

The VCI1 for the period 2000–2014 for the upper and middle part of the Tomebamba subbasin is shown in Fig. 4. A total of 32 events reflecting bad vegetation conditions were identified for monthly VCI's. The years 2001, 2003, 2007, 2008, 2012 and 2014 showed poor vegetation conditions (VCI<40%). About 70% of the analyzed months present good vegetation conditions. The most frequent month that shows bad conditions in vegetation was April. The month with the lowest VCI values was November. The year 2012 contained the highest amount of months with lowest VCI values (less than 40%).

3.4. Relationship between droughts and vegetation conditions

Wavelet coherence analysis was conducted to evaluate the strength of the relationship between SPI1–VCI1, VCI1–SSI1 and SPI1–SSI1 (Fig. 5). As a preliminary analysis, bi-monthly and three-monthly scales were also assessed in this study because most drought events had a duration from one to three months. However, the results were similar to the one-month scale, concerning the same periods and span of years with a highly significant correlation. In Fig. 5 are the significant consistencies (5% significance level) framed with a thick contour. Arrows with a left to right direction indicate that the indices are in phase; there is a positive relationship. Arrows with a right to left direction indicate a negative relationship (antiphase) (Lin et al., 2017). The influence cone is bounded by the white shaded area and indicates where the edge effects occur in the coherence data (Torrence and Compo, 1998).

Fig. 5a depicts the Wavelet Coherency obtained between the SPI1 and VCI1. In the 1.6 years, the best correlation was obtained between 2009 and 2012 with a coherence level around 0.8. The variables were out of phase, which means the correlation is negative. In addition, VCI1 had a delay between 1 and 1.5 months with SPI1. Between 2009 and 2012, five meteorological drought events occurred. The longest one (3 months) occurred between August and October 2009, with an average intensity of −1.32. The other events were monthly, and the most intense (−2.27) occurred in March 2011. In comparison, the VCI1 range indicates that vegetation

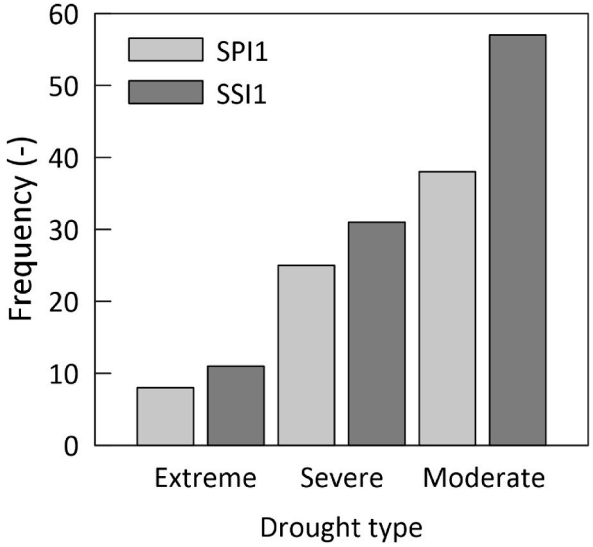

Fig. 3. Distribution of the monthly frequency of meteorological and hydrological drought events.

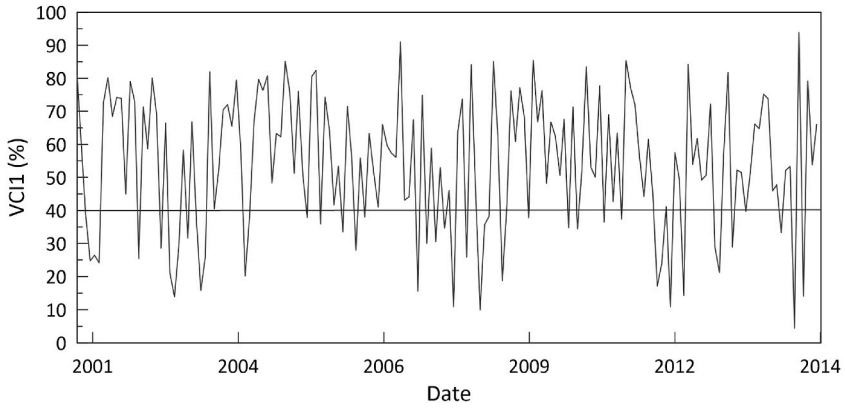

Fig. 4. Time series of the VCI1 for the period 2001–2014. The horizontal line indicates the threshold of good (VCI>40%) and stress (VCI<40%) condition of vegetation.

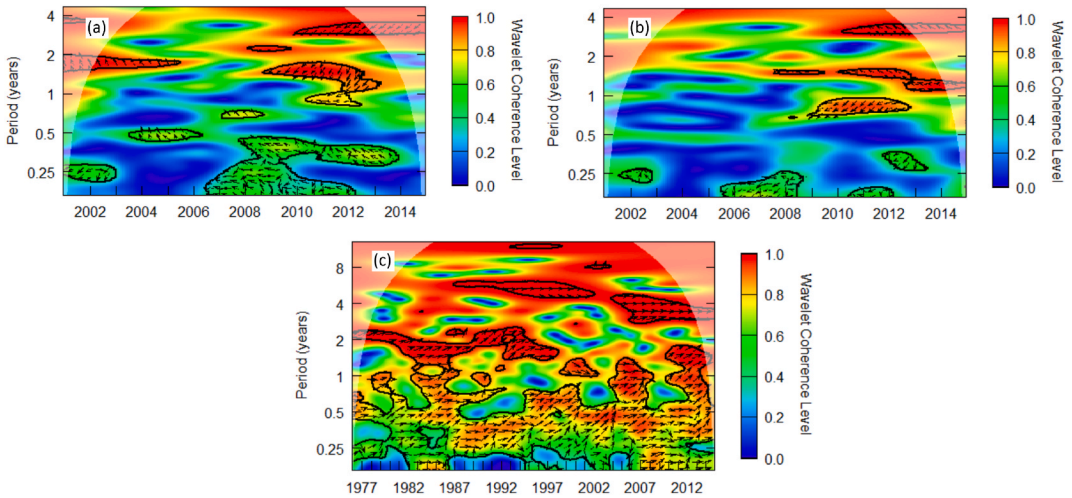

Fig. 5. Wavelet coherence between (a) SPI1 and VCI1, (b) VCI1 and SSI1, and (c) SPI1 and SSI1.

was predominantly in good condition. At lower periods, significant negative correlations were obtained; however, its values were lower than 0.5.

Fig. 5b shows the relationships between VCI1 and SSI1. The most relevant correlations (higher than 0.7) occurred around the period 0.8 and 1.2 years, both out of phase. Between 2010 and 2012, in the period ~1.6 years, a delay of VCI of approximately 0–2.5 months was found. On the other hand, in the period around 0.8 years, between 2009 and 2012, an advance of the VCI of ~1 month was observed. There were only three drought events of bimonthly duration and one of quarterly duration (July to Sep/2012). All of these events with an intensity of less than −1.5. During the lower periods (less than six months), the vegetation remains in optimal condition (VCI greater than 40%) most of the time despite the inverse relationship with SSI; only two drought events of monthly duration were registered.

Fig. 5c shows the relationship between SPI1 and SSI1. In approximately 3–7 years, a strong positive correlation greater than 0.9 (on average) was observed. Besides, a constant positive correlation was observed between the periods ~3–7 months (0.25–0.58 years). The period of 5 months (0.42 years) had the best average coherence (0.75), where SPI1 influences SSI1 with a delay ranging between zero and three weeks.

The relationships between the SPI1, SSI1 and VCI1 indices revealed that the vegetation is not entirely modified by the rain or the streamflow, unless extreme weather conditions occur. With streamflow, a varied antiphase behavior, which shows two scenarios, was identified; respectively, a scenario where the vegetation controls the flow rates and a second one where the changes in the flow rates affect the vegetation. In the first scenario, the streamflow decreases when the vegetation is in good condition; however, the effect is not drastic and does not generate significant hydrological drought events. In the second case, when relevant changes in streamflow occur not being the consequence of the condition of the vegetation, the increase in the number of hydrological drought events are linked to SPI1.

The relationship between drought and vegetation conditions is complex. Studies on the impact of drought on vegetation showed

significant spatial variability in the relationship between VCI and SPI (Rousta et al., 2020). The highest correlations were found in dry places (Şorman et al., 2018), farmland and grasslands (Vicente-Serrano, 2007), while humid areas with high permeability (Quiring and Ganesh, 2010), irrigation land and forests (Zou et al., 2020) showed weak correlations. The latter results agree with our findings in the Tomebamba subbasin which corresponds to a humid climate. The VCI was also evaluated with the discharge anomaly percentage index (PDA). Although the correlations are significant but weak, the VCI index shows a neutral trend as the PDA increases or decreases (Bandad and Rahmani, 2018).

For the páramo area, the vegetation's condition is only positively affected when moderate meteorological drought events lasting longer than three months occur. Under other conditions, the VCI index does not capture the reaction of the vegetation to meteorological changes. This result could be explained by the low performance of this remote sensing index for the biophysical and biochemical properties of the vegetation (Zou et al., 2020). Also, the páramo soils remain saturated, and several studies have shown weak correlations between VCI and droughts when the land cover and soil moisture conditions control vegetation's condition (Quiring and Ganesh, 2010; Şorman et al., 2018; Vicente-Serrano, 2007; Zou et al., 2020).

On the other hand, for the analysis of the influence of hydrological drought in the vegetation condition, it was found that the number of hydrological drought events is minimal when the vegetation condition is good (over 40%). However, based on the results of this study, when SPI1 generates sudden changes in the SSI1, the vegetation no longer controls the condition of the hydrological drought and SSI1 is subsequently affected. Also, by relating the two drought indices, a constant and robust correlation over time indicates that SPI1 can effectively predict changes in current streamflow.

3.5. Relationship between reanalysis data and SPI1, SSI1 and VCI1 indices

Reanalysis products are considered reference datasets for hydrological modeling, demonstrating that their performance using precipitation and temperature variables of ERA-5 is equivalent to the use of observations in a large area (Tarek et al., 2020). In some regions of China, meteorological drought indices and drought areas are even more representative when estimated from reanalysis data (Chen et al., 2019). It is important to note that not all reanalysis products have the same reliability and applicability for climate and hydrological studies. For example, in India, when using reanalysis data such as NCEP/NCAR Reanalysis (NCEP R1), NCEP-DOE AMIP-2 Reanalysis (NCEP R2), Climate Forecast System Reanalysis (CFSR), ECMWF Interim Reanalysis (ERA-Interim), Modern Era Retrospective Analysis for Research and Application Land only model (MERRA-Land) and JMA 55-year Reanalysis (JRA-55), researchers concluded that none of these products could correctly reproduce the precipitation and temperature trends (Ghodichore et al., 2018; Shah and Mishra, 2014). However, recently, ERA-5 has proven to be more functional than other products and gave in India evidence that it can be used effectively for hydrological assessments (Mahto and Mishra, 2019).

The best correlations between drought indices/vegetation condition index and reanalysis data sets for our study area were obtained at 500–750 hPa. At pressure levels lower or higher than the range mentioned above, the coherence between the analyzed variables is negligible.

Our study found the best correlations between reanalysis variables and SPI1 with the fraction of cloud cover at 500 hPa and relative humidity at 600 hPa (Fig. 6). Regarding the fraction of cloud cover, an average positive correlation of 0.95 was observed between 5 and 6 years, where the series did not present significant delays between them, and the SPI1 is less than one month ahead. The positive relationship between the fraction of cloud cover and the SPI1 indicates that the reduction in cloud cover is linked to drought events. These results are similar to previous studies carried out in tropical South America using reanalysis data (Campozano et al., 2016; Jimenez et al., 2018) or using other types of satellite data (Butt et al., 2009; Martins et al., 2018; Salazar et al., 2007). These studies claim that total cloud cover tends to decrease in the dry season and increase in the wet season.

For the relative humidity, the correlation is also positive with a delay of SPI1 between 0 and 3 months around 5-year intervals in 1985–1997. These results agree with Behrangi et al. (2016), who indicated that the relative humidity decreases during the formation and intensification of dry events. The concurrence of abnormally high temperatures and low humidity has also been found to be an essential driver of the rapid development and evolution of droughts (Behrangi et al., 2015).

At lower periods for both atmospheric variables, between 0.25 and 0.5 years is the average correlation ~0.5. However, the phase between the series is unclear, finding time lapses in periods where the SPI1 is delayed or advanced concerning the fraction of cloudiness and relative humidity.

The best correlations with SSI1 were obtained with the fraction of cloud cover at 500 hPa, relative humidity at 750 hPa, and temperature at 600 hPa (Fig. 7). The results are similar to those obtained with SPI (Fig. 6). For the first two reanalysis variables, for

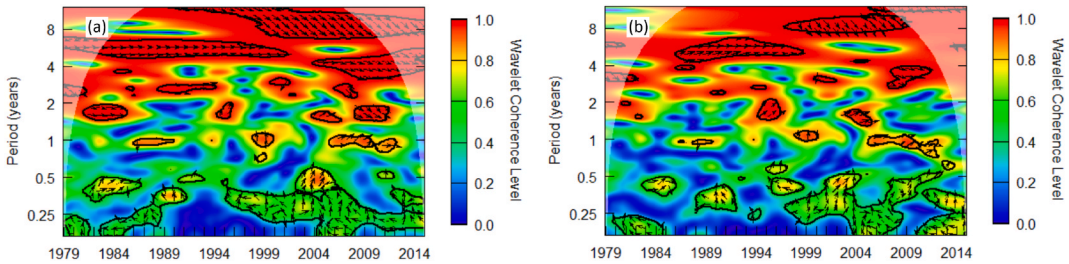

Fig. 6. Wavelet Coherence between SPI1 and a) fraction of cloud cover 500 hPa, and b) relative humidity 600 hPa.

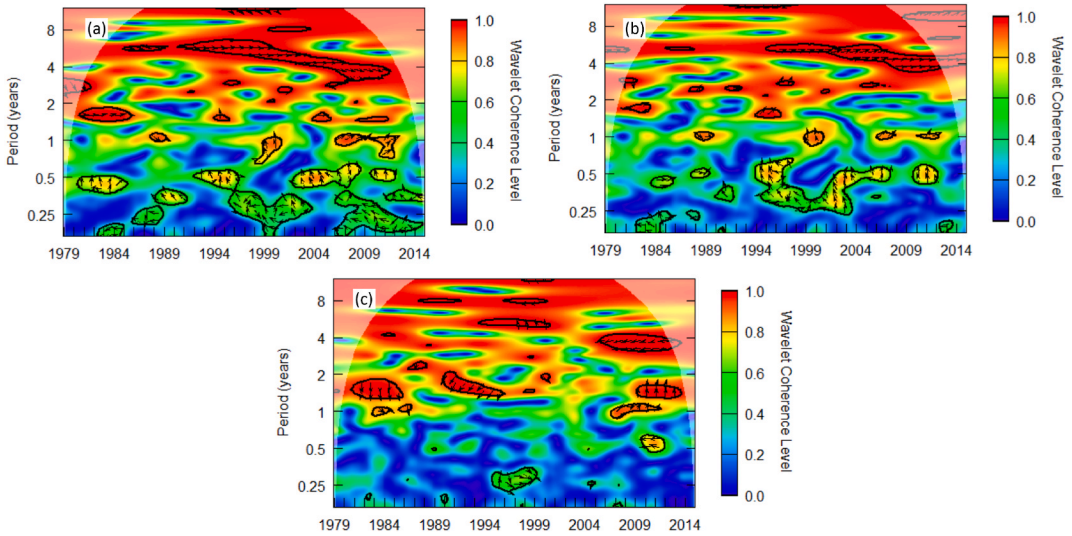

Fig. 7. Wavelet Coherence between SSI1 and a) the fraction of cloud cover 500 hPa, b) relative humidity 750 hPa, and c) temperature 600 hPa.

periods between 4 and 6 years, the correlations were positive, more significant than 0.9, with an advance (delay) of SSI1 between 0 and 1 month concerning the fraction of cloudiness (relative humidity). For temperature, the highest coherence levels (~0.9) occur between 1 and 2 years, being negative during 1980–1985, 1989–1995, and positive during 2008–2013, with an SSI1 delay between 2 and 4 months. Considering only the period where hydrological drought events occurred, it was observed that the air temperature at 600 hPa increased. Studies carried out in southwestern Europe and on a global scale have linked extreme hot temperatures to precipitation deficit, showing that the probability of hot extremes is linked to the scarcity of rain (Hirschi et al., 2011; Mueller and Seneviratne, 2012). In China and Iran, where the relationship between precipitation and surface temperature has been studied, it was identified that water deficits are generally associated with high temperatures (He et al., 2015), as well as that trends for temperature are increasing, while for rainfall decreasing (Bazrafshan, 2017).

The best correlations for the reanalysis data and VCI1 were obtained with the specific rain content at 650 hPa and specific humidity at 700 hPa (Fig. 8). For the specific content of rain, a negative relationship was obtained, in the ~2-year period, from 2006 to 2012, with a delay in VCI1 of fewer than 1.5 months. Another negative correlation of ~0.7 stands out in the period around 0.3 years during 2010–2013, with a delay in VCI1 of less than one month. Regarding specific humidity, a positive correlation of ~0.9 was observed around the two years during 2009–2012, with an advance of ~ three months of VCI1. At lower periods, a correlation was found in 6 months (2002–2005) and 3.6 months (2010–2013); both correlations are negative with a coherence level of ~0.7 and ~0.6, respectively, and a delay in VCI1 between 1 and 2 months. These results suggest that the increase in the specific content of rain and specific humidity could negatively affect the condition of the vegetation (range less than 40%). Fu and Shen (2016) found similar results in their study, concluding that environmental humidity conditions and precipitation significantly affect the vegetation index and biomass production of the alpine grasslands on the Tibetan Plateau. However, Muradyan et al. (2019) found positive correlations between vegetation conditions and precipitation in mountains ecosystems in Armenia. Also, a strong positive correlation of vegetation in Iran with other atmospheric factors such as cloud fraction has been found (Ghasemifar et al., 2018).

3.6. Relationship between large-scale climatic indices and SPI1, SSI1 and VCI1 indices

Research about drought development recognized that changes in global ocean temperature or large-scale climatic factors could be crucial for drought development (Lin et al., 2017). Therefore, the relationships between the severity of the different droughts and the leading climatic indices were examined using the Wavelet Coherence Analysis.

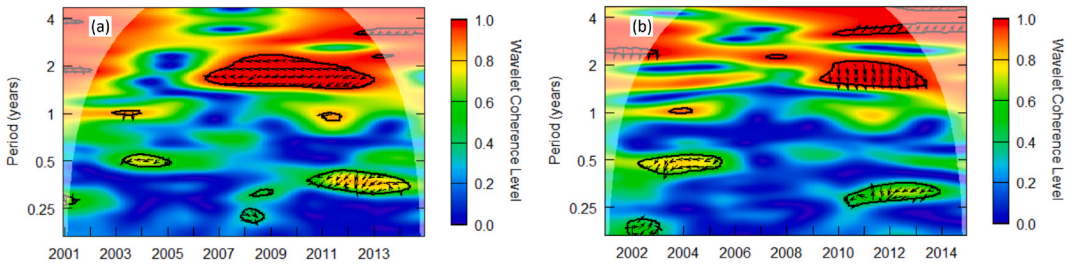

Fig. 8. Wavelet Coherence between VCI1 and a) specific rainwater content at 650 hPa and b) specific humidity at 700 hPa.

The correlations between the 15 climatic indices and the SPI1 indicated that the best relations occur with MEI, ENSO 3, SOI, PNA and PDO (Fig. 9). Relationships were also found with other indices associated with ENSO; however, only the best results are reported. In general, the correlations found with the indices associated with the ENSO phenomenon coincide in time-frequency. The most appropriate coherence levels were found between 3 and 7 years. During 1990–2001 for periods between 5 and 7 years, a positive correlation was observed between SPI1 with MEI, ENSO 3, and SOI indices. Concerning MEI and ENSO 3, correlations were observed around four years between 1981 and 1988, 2009–2012. The variables were in phase (positive correlation) in the first period, with a SPI1 delay of approximately ten months. The relationship changed to antiphase (negative correlation) with a SPI1 delay of 4 months in the second period. Besides, for the period between 5 and 7 years, the relationship was positive during ~1990–2001, with a SPI1 delay of ~15 months.

Regarding SOI, similar results as MEI and ENSO 3 indices were found in the same time-frequency span. However, a difference in the phase change was observed. The relationship is negative in the four years between 1981 and 1988, with a delay of the SPI1 of approximately one year. In contrast, the relationship is positive between 2009 and 2012, with a delay of the SPI1 of ~ five months. Other indices, such as ENSO 4, ENSO 3.4 and ONI showed a correlation in time-frequency; however, the level of coherence is slightly lower. The results agree with those reported by Ávila and Ballari (2020), who found that the leading climatic indices that affect precipitation in the southern Andean region of Ecuador are: ENSO 1 + 2, MEI, ENSO 4, and ONI. Also, the influence of ENSO 1 + 2 and TSA on the variability of local rainfall has been reported, particularly in the dry months within the study area (Mora et al., 2014). Besides, the positive relation between the MEI index and meteorological droughts coincides with other world areas (Tadesse et al., 2004; Wang et al., 2019); however, it is against with results of other authors (Ganguli and Janga Reddy, 2013; Shahid, 2008). These contradictions were to be expected since the influence of ENSO is different in various parts of the world (Sun et al., 2015).

In comparison with similar studies in Andean basins, for example, in the southern Peruvian Andes, it was found that rainfall decreases during an intense El Niño event and increases during a strong La Niña event (Lavado and Espinoza, 2014). Besides, in Cali (Colombia), it was found that macroclimatic variables such as ONI and MEI have the most significant influence on the precipitation and streamflow variables (Cerón et al., 2020). It was highlighted that the influence in streamflow by the ENSO ($r = -0.44$) is primarily due to the process of water storage in aquifers, or the conditions of antecedent humidity in the soil; which generated a historical memory in the streamflow series (Ávila Díaz et al., 2014). Other studies have found relationships between rainfall in South America and the ENSO phenomenon. These indicate that El Niño warm phase is undoubtedly associated with the meteorological droughts of northern South America, including the Amazon rainforest, while La Niña cold phase affects the South of the continent (Bento et al., 2019).

Relationships were also found with indices associated with the North Pacific, PNA and PDO. The following relevant relationships were found with PNA: in the period of about 1.5 years, during 1990–1991 negative with a delay of ~ two months; in the period of 4.5

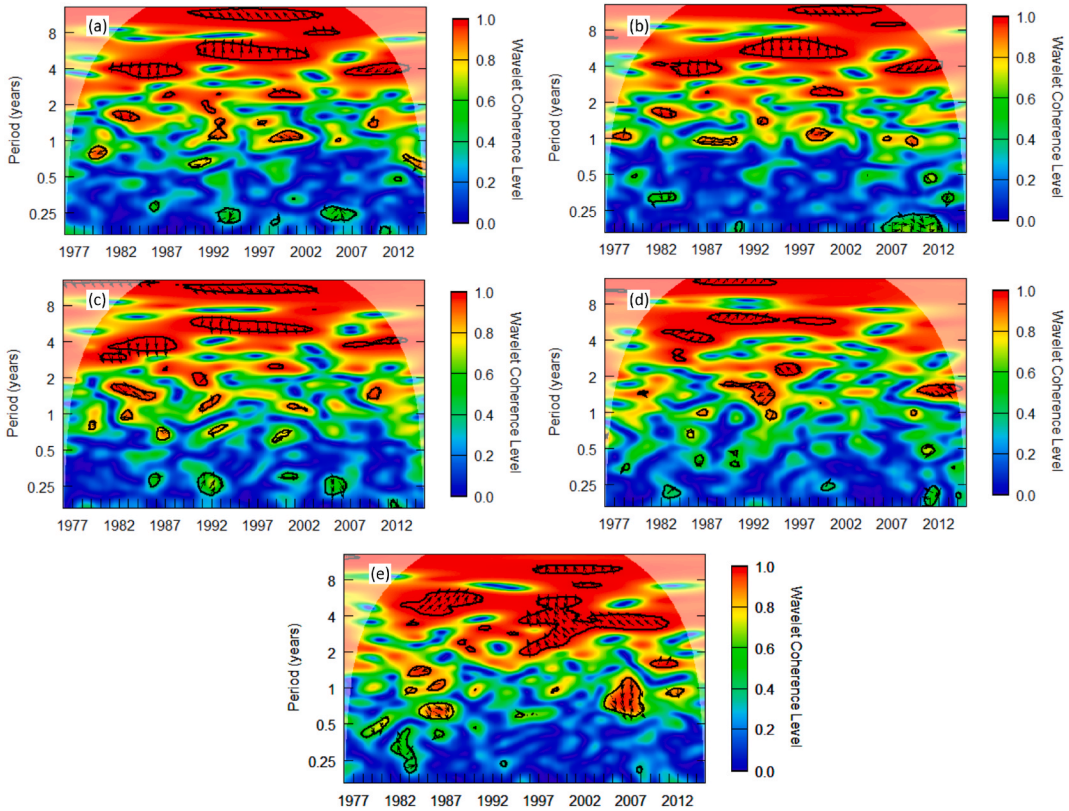

Fig. 9. Wavelet coherence between SPI1 and a) MEI, b) ENSO 3, c) SOI, d) PNA, and e) PDO.

years, during 1982–1988 positive with a delay of ~ six months; and in the period ~6 years, 1989–2000 positive with a delay of ~ nine months. With PDO, better correlations were found between periods 3-7 years since 1981, where the correlations were positive before 1997; later, a progressive phase change with a negative correlation was observed. From that year onwards, the correlation remained strong until 2012. The phase angle to determine a time of delay or advance is not entirely defined, and this may be due to the intermediate phase variations of PDO between 1998 and 2010. This index is positive when the temperature is abnormally warm, like along the coast of North America, Central America and Ecuador, and cold in the Central North Pacific (Trenberth and Hurrell, 1994).

There are some coincidences in the correlated time between SPI1 with PDO, PNA and the indices associated with ENSO; as other authors mentioned, PDO can modulate the relationship of ENSO in different regions (Córdoba-Machado et al., 2016; Oñate-Valdivieso et al., 2020). Campozano et al. (2020b) determined that PDO influences the relationship between ENSO and rainfall in the Ecuadorian coastal region. Besides, PNA phases are associated with the phase state of ENSO and PDO (Trouet and Taylor, 2010).

The relationships between the 15 climatic indices and SSI1 were analyzed. In general, MEI, ENSO 3, ENSO 3.4, ENSO 4, ONI, and SOI indices show similar correlations. ENSO 4 index stands out among them, as shown in Fig. 10. It is observed that the correlated indices are similar to those found for SPI1. The periods with the best correlations for ENSO 4 are: 1 year (between 1999 and 2000) with a negative relationship and delayed SSI1 ~3 months; 1.5 years (between 1994 and 1995) with a negative relationship and delay of ~ five months; and 3.5 years (between 2005 and 2010) with a negative relationship and delay of ~ one month.

Studies about the relations between climatic phenomena such as ENSO and the Paute river basin's hydrology (in Ecuador) show significant relationships between such variables (Hoorelbeke et al., 2000). In 1999, it was shown that El Niño did affect the distribution of monthly streamflow in Amazon basins. Besides, it was stated that annual volumes that enter the Amaluza reservoir are significantly correlated with the anomalies of sea surface temperature (SST) in the regions ENSO 1 + 2, in the La Niña phase. Moreover, Quishpe-Vásquez et al. (2019) indicated the significant relationship between ENSO 4 and the streamflow during dry months (June–August) in several locations of the Andes in Ecuador.

The coherence between the VCI1 series and the leading climatic indices was analyzed. In general, the results revealed the existence of minimal correlations with all the indices, highlighting the consistency with the PNA index, as shown in Fig. 10. The PNA index had the best correlation, but the correlation areas are scarce even so. The correlation was negative during 2007–2009 (2,5-years period) with a lag of less than one month and during 2008–2011 (the period between 1 and 2 years) but with lags of ~ two months. The short periods can limit establishing deeper relationships between vegetation and climatic indices. Therefore, it is necessary to extend the VCI1 time series in future studies, or instead, to test other vegetation indexes in order to find the one that best fits the evaluated area.

3.7. *Uncertainties and implications of this study*

Based on the results reported in the previous sections, we identify some aspects of uncertainty in this study. Firstly, the scarce availability of meteorological stations in the study area inhibits proper characterization of meteorological droughts' spatial and temporal variability. Although the dynamic variations of meteorological drought were identified in the Tomebamba basin, in order to recognize the drought phenomenon more clearly, other meteorological variables (e.g., temperature, relative humidity, solar radiation and wind speed) based on remote sensing information should be considered in the future. Secondly, the performance of VCI used to represent vegetation conditions (emulating agricultural droughts) in the study area strongly affects our findings. Further studies are required to identify the best index to study the variability of soil moisture and vegetation in mountain ecosystems such as páramo, such as water-related indexes that represent better the hydrologic cycle (Liou et al., 2019). Third, we only used a coherency wavelet to study the propagation and relation of droughts with meteorological and climatic factors. In order to corroborate our findings, it could be interesting to compare the results of other commonly used methods such as Pearson and Spearman correlation. Additionally, the drought process is complex and may be simultaneously affected by more than one driver (e.g., local/regional atmospheric conditions and large-scale climate indices), which requires the exploration of coupled effects of multiple factors on drought. For a better understanding of the drought process, multivariate analysis employing novel techniques such as the multivariate cross wavelet is required (Wang et al., 2022).

4. Conclusions

The fundamental part of this study corresponds to the analysis of relationships between meteorological and hydrological droughts and the condition of the vegetation, and in turn with atmospheric variables at the local scale and large-scale climatic indices. For this purpose, the wavelet coherence method was used. Our study provides valuable knowledge about the propagation of droughts and the

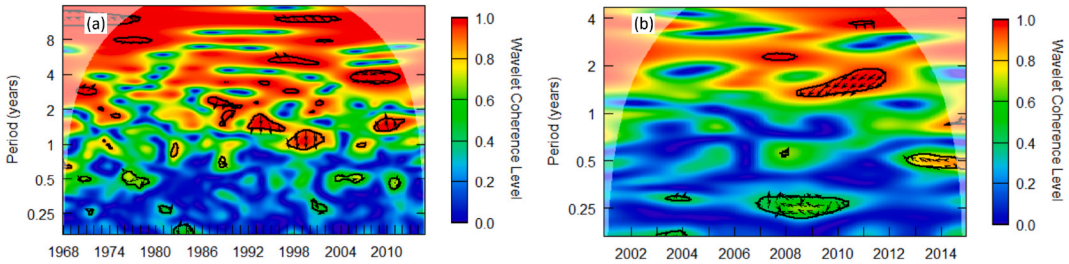

Fig. 10. Wavelet coherence between (a) ENSO 4 and SSI1 and (b) PNA and VCI1.

identification of drivers that influence droughts in the study area and the region. The principal findings of this study are listed below.

1) Concerning the relationships between droughts types and vegetation conditions, it was shown that the vegetation modulates flows as long as there are no abrupt changes in precipitation when analysing the relationships with hydrological drought. Thus, when VCI1 remains above 40%, there are few short duration and low severity hydrological drought events. Still, when there are marked variations in precipitation, a direct affectation occurs first to the flows and later to the vegetation. Besides, we found a solid and constant relationship throughout the analyzed period between SPI1 and SSI1.
2) The relationships of SPI1, SSI1 and VCI1 with the atmospheric variables at the local scale revealed that dry events are associated with atmospheric conditions between 500 and 750 hPa, with a decrease in the fraction of cloud cover and relative humidity and an increase in temperature. When the vegetation is in bad condition, it is associated with increased specific rainwater content and specific humidity.
3) Respectively, for the relationships between climatic indices and the meteorological and hydrological droughts, it was found that the best indices are MEI, ENSO 3, ENSO 3.4, ENSO 4, ONI and SOI. All of them were associated with ENSO. Among those mentioned, ENSO 4 stands out regarding hydrological drought, while MEI, SOI, and ENSO 3 highlight better correlations with SPI1. A scale correlation was also obtained for PDO and PNA with the SPI1. The influence on the precipitation was attributed to the phase changes of PDO in 1997 and in the following years until ~2010. The PNA and PDO show associations that partially coincide with the indices related to ENSO, which suggests the interconnection and modulation between these climatic factors.
4) Relationships between the VCI1 and climatic indexes did not show good results; PNA is the index with the higher relationship. None of the indices associated with ENSO influenced the condition of the vegetation. These results may be imprecise due to the short period of analysis, limitations of the satellite data for the calculation of the VCI, or to the low performance of the VCI for describing the state of the vegetation in an area that contains land use such as páramo (high elevation wetlands). It is recommended to characterize the vegetation employing other indices that better fit the study area for future studies.
5) The high and consistent relationship of SPI1 and SSI1 indicates a high potential to predict hydrological droughts based on meteorological droughts in the study area. More importantly, large-scale climate indices that show high relationships at high lag times could be suitable for the basin's drought early warning systems.

Funding

This work was supported by the University of Cuenca through its Research Department (DIUC) as part of the project titled "Estudio de las condiciones climatológicas de América del Sur que producen las sequías en el Ecuador continental".

Ethical Statement

Hereby, I Alex Avilés (Corresponding author) and on behalf of my co-authors, consciously assure that for the manuscript "Assessment of drought time-frequency relationships with local atmospheric-land conditions and large-scale climatic factors in a tropical Andean basin" the following is fulfilled:

1) This material is the authors' own original work, which has not been previously published elsewhere.
2) The paper is not currently being considered for publication elsewhere.
3) The paper reflects the authors' own research and analysis in a truthful and complete manner.
4) The paper properly credits the meaningful contributions of co-authors.
5) The results are appropriately placed in the context of prior and existing research.
6) All sources used are properly disclosed (correct citation).
7) All authors have been personally and actively involved in substantial work leading to the paper, and will take public responsibility for its content.

The violation of the Ethical Statement rules may result in severe consequences.

I agree with the above statements and declare that this submission follows the policies of Remote Sensing Applications: Society and Environment as outlined in the Guide for Authors.

Authorship contributions

A. Nieves, Conception and design of study, Analysis and/or interpretation of data, Methodology and software, Drafting the manuscript, Approval of the version of the manuscript to be published, J.Contreras, Acquisition of data, Analysis and/or interpretation of data, Methodology and software, Drafting the manuscript, Approval of the version of the manuscript to be published, J. Pacheco, Acquisition of data, Analysis and/or interpretation of data, Drafting the manuscript, Approval of the version of the manuscript to be published, J. Urgilés, Analysis and/or interpretation of data, Methodology and software, Drafting the manuscript, Approval of the version of the manuscript to be published, A.Avilés: Conception and design of study, Analysis and/or interpretation of data, Drafting the manuscript, Writing -Reviewing and Editing, Supervision, Approval of the version of the manuscript to be published, F.García: Acquisition of data, Writing -Reviewing and Editing, Approval of the version of the manuscript to be published.

Declaration of competing interest

The authors declare that they have no known competing financial interests or personal relationships that could have appeared to

influence the work reported in this paper.

Acknowledgements

Thanks to INAMHI and ETAPA for providing the information on the hydrological and rain gauge stations. Many thanks to Jan Feyen for his support in revising the manuscript.

References

Alvarenga, L.A., de Mello, C.R., Colombo, A., Cuartas, L.A., Bowling, L.C., 2016. Assessment of land cover change on the hydrology of a Brazilian headwater watershed using the Distributed Hydrology-Soil-Vegetation Model. Catena 143, 7–17. https://doi.org/10.1016/j.catena.2016.04.001.

Aquino, D.S., Gavier-Pizarro, G., Quintana, R.D., 2021. Disentangling the effects of hydro-climatic factors and land use intensification on wetland vegetation dynamics in the Lower Delta of the Paraná River. Remote Sens. Appl. Soc. Environ. 21, 100466 https://doi.org/10.1016/j.rsase.2021.100466.

Ávila Díaz, Á.J., Carvajal Escobar, Y., Gutiérrez Serna, S.E., 2014. Análisis de la influencia de El Niño y La Niña en la oferta hídrica mensual de la cuenca del río Cali. Tecnura 18, 120–133.

Ávila, R., Ballari, D., 2020. A bayesian network approach to identity climate teleconnections within homogeneous precipitation regions in Ecuador. In: Fosenca C, E., Rodríguez Morales, G., Orellana Cordero, M., Botto-Tobar, M., Crespo Martínez, E., Patiño León, A. (Eds.), Information and Communication Technologies of Ecuador (TIC.EC). Springer International Publishing, Cham, pp. 21–35.

Avilés, A., Célleri, R., Paredes, J., Solera, A., 2015. Evaluation of Markov chain based drought Forecasts in an andean regulated river basin using the skill scores RPS and GMSS. Water Resour. Manag. 29 https://doi.org/10.1007/s11269-015-0921-2.

Avilés, A., Célleri, R., Solera, A., Paredes, J., 2016. Probabilistic forecasting of drought events using Markov chain- and bayesian network-based models: a case study of an andean regulated river basin. Water 8, 37. https://doi.org/10.3390/w8020037.

Baek, S.H., Smerdon, J.E., Coats, S., Williams, A.P., Cook, B.I., Cook, E.R., Seager, R., 2017. Precipitation, temperature, and teleconnection signals across the combined North American, monsoon Asia, and old world drought atlases. J. Clim. 30, 7141–7155. https://doi.org/10.1175/JCLI-D-16-0766.1.

Ballari, D., Campozano, L., Samaniego, E., Orellana, D., 2020. Spatial association to characterize the climate teleconnection patterns in Ecuador based on satellite precipitation estimates. IEEE Lat. Am. GRSS ISPRS Remote Sens. Conf. LAGIRS 2020 - Proc. 219–224. https://doi.org/10.1109/LAGIRS48042.2020.9165647, 2020.

Bandad, D., Rahmani, V., 2018. Analysis of PDSI and vegetation condition index (VCI) and their links to streamflow. In: American Society of Agricultural and Biological Engineers Annual International Meeting. American Society of Agricultural and Biological Engineers, Michigan, pp. 1–7.

Barnston, A.G., Livezey, R.E., 1987. Classification, Seasonality and Persistence of Low-Frequency Atmospheric Circulation Patterns. Montly Weather Rev. https://doi.org/10.1175/1520-0493(1987)115<1083:csapol>2.0.co:2.

Bazrafshan, J., 2017. Effect of air temperature on historical trend of long-term droughts in different climates of Iran. Water Resour. Manag. 31, 4683–4698. https://doi.org/10.1007/s11269-017-1773-8.

Behrangi, A., Fetzer, E.J., Granger, S.L., 2016. Early detection of drought onset using near surface temperature and humidity observed from space. Int. J. Rem. Sens. 37, 3911–3923. https://doi.org/10.1080/01431161.2016.1204478.

Behrangi, A., Loikith, P.C., Fetzer, E.J., Nguyen, H.M., Granger, S.L., 2015. Utilizing humidity and temperature data to advance monitoring and prediction of meteorological drought. Climate 3, 999–1017. https://doi.org/10.3390/cli3040999.

Bendix, J., Rollenbeck, R., Göttlicher, D., Cermak, J., 2006. Cloud occurrence and cloud properties in Ecuador. Clim. Res. 30, 133–147. https://doi.org/10.3354/cr030133.

Bento, V., Libonati, R., Gouveia, C., DaCamara, C., 2019. Understanding the impact of ENSO-related droughts over South American vegetation health. Geophys. Res. Abstr.

Berghuijs, W., Sivapalan, M., Woods, R., Savenije, H., 2014. Patterns of similarity of seasonal water balances: a window into streamflow variability over a range of time scales. Water Resour. Res. 50, 5375–5377. https://doi.org/10.1002/2013WR014979.Reply.

Bonnesoeur, V., Locatelli, B., Guariguata, M.R., Ochoa-Tocachi, B.F., Vanacker, V., Mao, Z., Stokes, A., Mathez-Stiefel, S.L., 2019. Impacts of forests and forestation on hydrological services in the Andes: a systematic review. For. Ecol. Manage. 433, 569–584. https://doi.org/10.1016/j.foreco.2018.11.033.

Brassel, K.E., 1979. Procedure to generate thiessen polygons. Geogr. Anal. 11.

Butt, N., New, M., Lizcano, G., Malhi, Y., 2009. Spatial patterns and recent trends in cloud fraction and cloud-related diffuse radiation in Amazonia. J. Geophys. Res. Atmos. 114 https://doi.org/10.1029/2009JD012217.

Buytaert, W., Célleri, R., De Bièvre, B., Cisneros, F., Wyseure, G., Deckers, J., Hofstede, R., 2006. Human impact on the hydrology of the Andean páramos. Earth Sci. Rev. 79, 53–72. https://doi.org/10.1016/j.earscirev.2006.06.002.

Campozano, L., Ballari, D., Montenegro, M., Avilés, A., 2020a. Future meteorological droughts in Ecuador: decreasing trends and associated spatio-temporal features derived from CMIP5 models. Front. Earth Sci. 8 https://doi.org/10.3389/feart.2020.00017.

Campozano, L., Célleri, R., Trachte, K., Bendix, J., Samaniego, E., 2016. Rainfall and cloud dynamics in the Andes: a southern Ecuador case study. Adv. Meteorol. 2016.

Campozano, L., Robaina, L., Samaniego, E., 2020b. The Pacific Decadal Oscillation modulates the relation of ENSO with the rainfall variability in coast of Ecuador. Int. J. Climatol. 40 https://doi.org/10.1002/joc.6525.

Campozano, L., Trachte, K., Célleri, R., Samaniego, E., Bendix, J., Albuja, C., Mejia, J.F., 2018. Climatology and teleconnections of mesoscale convective systems in an Andean basin in southern Ecuador: the case of the Paute basin. Adv. Meteorol. https://doi.org/10.1155/2018/4259191, 2018.

Carlson, T.N., Arthur, S.T., 2000. The impact of land use—land cover changes due to urbanization on surface microclimate and hydrology: a satellite perspective. Global Planet. Change 25, 49–65.

Casa, A. de la, Ovando, G., Díaz, G., 2021. Linking data of ENSO, NDVI-MODIS and crops yield as a base of an early warning system for agriculture in Córdoba, Argentina. Remote Sens. Appl. Soc. Environ. 22, 100480 https://doi.org/10.1016/j.rsase.2021.100480.

Célleri, R., Feyen, J., 2009. The hydrology of tropical andean ecosystems: importance, knowledge status, and perspectives. Mt. Res. Dev. 29, 350–355. https://doi.org/10.1659/mrd.00007.

Cerón, W.L., Carvajal-Escobar, Y., De Souza, R.V.A., Kayano, M.T., López, N.G., 2020. Spatio-temporal analysis of the droughts in Cali, Colombia and their primary relationships with the El Nino-Southern Oscillation (ENSO) between 1971 and 2011. Atmósfera 33, 51–69. https://doi.org/10.20937/ATM.52639.

Chen, S., Gan, T.Y., Tan, X., Shao, D., Zhu, J., 2019. Assessment of CFSR, ERA-Interim, JRA-55, MERRA-2, NCEP-2 reanalysis data for drought analysis over China. Clim. Dynam. 53, 737–757. https://doi.org/10.1007/s00382-018-04611-1.

Choat, B., Jansen, S., Brodribb, T.J., Cochard, H., Delzon, S., Bhaskar, R., Bucci, S.J., Feild, T.S., Gleason, S.M., Hacke, U.G., Jacobsen, A.L., Lens, F., Maherali, H., Martínez-Vilalta, J., Mayr, S., Mencuccini, M., Mitchell, P.J., Nardini, A., Pittermann, J., Pratt, R.B., Sperry, J.S., Westoby, M., Wright, I.J., Zanne, A.E., 2012. Global convergence in the vulnerability of forests to drought. Nature 491, 752–755. https://doi.org/10.1038/nature11688.

Cincotta, R.P., Wisnewski, J., Engelman, R., 2000. Human population in the biodiversity hotspots. Nature. https://doi.org/10.1038/35010105.

Córdoba-Machado, S., Palomino-Lemus, R., Gámiz-Fortis, S.R., Castro-Díez, Y., Esteban-Parra, M.J., 2016. Seasonal streamflow prediction in Colombia using atmospheric and oceanic patterns. J. Hydrol. 538, 1–12. https://doi.org/10.1016/j.jhydrol.2016.04.003.

Crausbay, S.D., Ramirez, A.R., Carter, S.L., Cross, M.S., Hall, K.R., Bathke, D.J., Betancourt, J.L., Colt, S., Cravens, A.E., Dalton, M.S., Dunham, J.B., Hay, L.E., Hayes, M.J., McEvoy, J., McNutt, C.A., Moritz, M.A., Nislow, K.H., Raheem, N., Sanford, T., 2017. Defining ecological drought for the twenty-first century. Bull. Am. Meteorol. Soc. https://doi.org/10.1175/BAMS-D-16-0292.1.

Dalezios, N.R., Loukas, A., Vasiliades, L., Liakopoulos, E., 2000. Severity-duration-frequency analysis of droughts and wet periods in Greece. Hydrol. Sci. J. 45, 751–769.
Ding, Y., Gong, X., Xing, Z., Cai, H., Zhou, Z., Zhang, D., Sun, P., Shi, H., 2021. Attribution of meteorological, hydrological and agricultural drought propagation in different climatic regions of China. Agric. Water Manag. 255, 106996 https://doi.org/10.1016/j.agwat.2021.106996.
Dracup, J.A., Lee, K.S., Paulson, E.G., 1980. On the definition of droughts. Water Resour. Res. 16, 297–302. https://doi.org/10.1029/WR016i002p00297.
Dutta, D., Kundu, A., Patel, N.R., Saha, S.K., Siddiqui, A.R., 2015. Assessment of agricultural drought in Rajasthan (India) using remote sensing derived vegetation condition index (VCI) and standardized precipitation index (SPI). Egypt. J. Remote Sens. Sp. Sci. 18, 53–63. https://doi.org/10.1016/j.ejrs.2015.03.006.
Ebdon, R.A., 1960. Notes on the wind flow at 50 mb in tropical and sub-tropical regions in January 1957 and January 1958. Q. J. R. Meteorol. Soc. 86, 540–542.
Enfield, D.B., Mestas-Nuñez, A.M., Mayer, D.A., Cid-Serrano, L., 1999. How ubiquitous is the dipole relationship in tropical Atlantic sea surface temperatures? J. Geophys. Res. Ocean. 104, 7841–7848. https://doi.org/10.1029/1998jc900109.
Esquivel-Hernández, G., Mosquera, G.M., Sánchez-Murillo, R., Quesada-Román, A., Birkel, C., Crespo, P., Célleri, R., Windhorst, D., Breuer, L., Boll, J., 2019. Moisture transport and seasonal variations in the stable isotopic composition of rainfall in Central American and Andean Páramo during El Niño conditions (2015–2016). Hydrol. Process. 33, 1802–1817. https://doi.org/10.1002/hyp.13438.
Fleig, A.K., Tallaksen, L.M., Hisdal, H., Demuth, S., 2006. A global evaluation of streamflow drought characteristics. Hydrol. Earth Syst. Sci. 10, 535–552. https://doi.org/10.5194/hess-10-535-2006.
Flores-López, F., Galaitsi, S.E., Escobar, M., Purkey, D., 2016. Modeling of Andean Páramo Ecosystems' Hydrological Response to Environmental Change. Water (Switzerland), 8. https://doi.org/10.3390/w8030094.
Fu, G., Shen, Z.X., 2016. Environmental humidity regulates effects of experimental warming on vegetation index and biomass production in an alpine meadow of the northern tibet. PLoS One 11, e0165643. https://doi.org/10.1371/journal.pone.0165643.
Ganguli, P., Janga Reddy, M., 2013. Analysis of ENSO-based climate variability in modulating drought risks over western Rajasthan in India. J. Earth Syst. Sci. 122, 253–269. https://doi.org/10.1007/s12040-012-0247-x.
Gebrehiwot, T., van der Veen, A., Maathuis, B., 2011. Spatial and temporal assessment of drought in the Northern highlands of Ethiopia. Int. J. Appl. Earth Obs. Geoinf. 13, 309–321. https://doi.org/10.1016/j.jag.2010.12.002.
Ghasemifar, E., Farajzadeh, M., Perry, M.C., Rahimi, Y.G., Bidokhti, A.A., 2018. Analysis of spatiotemporal variations of cloud fraction based on geographic characteristics over Iran. Theor. Appl. Climatol. 134, 1429–1445. https://doi.org/10.1007/s00704-017-2308-1.
Ghodichore, N., Vinnarasi, R., Dhanya, C.T., Roy, S.B., 2018. Reliability of reanalyses products in simulating precipitation and temperature characteristics over India. J. Earth Syst. Sci. 127, 115. https://doi.org/10.1007/s12040-018-1024-2.
Gómez-Limón, J.A., 2020. Hydrological drought insurance for irrigated agriculture in southern Spain. Agric. Water Manag. 240, 106271 https://doi.org/10.1016/j.agwat.2020.106271.
Grinsted, A., Moore, J.C., Jevrejeva, S., 2004. Application of cross wavelet transform and wavelet coherence to geophysical time series. Nonlinear Process Geophys. 11 https://doi.org/10.5194/npg-11-561-2004.
Guo, Y., Huang, S., Huang, Q., Wang, H., Wang, L., Fang, W., 2019. Copulas-based bivariate socioeconomic drought dynamic risk assessment in a changing environment. J. Hydrol. 575, 1052–1064. https://doi.org/10.1016/j.jhydrol.2019.06.010.
Hao, Z., Singh, V.P., 2015. Drought characterization from a multivariate perspective: a review. J. Hydrol. 527, 668–678. https://doi.org/10.1016/j.jhydrol.2015.05.031.
He, B., Wang, H.L., Wang, Q.F., Di, Z.H., 2015. A quantitative assessment of the relationship between precipitation deficits and air temperature variations. J. Geophys. Res. Atmos. 120, 5951–5961. https://doi.org/10.1002/2015JD023463.
Hirschi, M., Seneviratne, S.I., Alexandrov, V., Boberg, F., Boroneant, C., Christensen, O.B., Formayer, H., Orlowsky, B., Stepanek, P., 2011. Observational evidence for soil-moisture impact on hot extremes in southeastern Europe. Nat. Geosci. 4, 17–21. https://doi.org/10.1038/ngeo1032.
Hoorelbeke, R., Calvez, R., Pombosa, R., Roura, J., García, F., Tejada, M., 2000. Modelización hidrológica en la cuenca del río Paute.
Huang, S., Huang, Q., Chang, J., Leng, G., Xing, L., 2015. The response of agricultural drought to meteorological drought and the influencing factors: a case study in the Wei River Basin, China. Agric. Water Manag. 159, 45–54. https://doi.org/10.1016/j.agwat.2015.05.023.
Javed, T., Yao, N., Chen, X., Suon, S., Li, Y., 2020. Drought evolution indicated by meteorological and remote-sensing drought indices under different land cover types in China. Environ. Sci. Pollut. Res. 27, 4258–4274. https://doi.org/10.1007/s11356-019-06629-2.
Jiang, T., Su, X., Singh, V.P., Zhang, G., 2022. Spatio-temporal pattern of ecological droughts and their impacts on health of vegetation in Northwestern China. J. Environ. Manag. 305, 114356 https://doi.org/10.1016/J.JENVMAN.2021.114356.
Jimenez, J.C., Libonati, R., Peres, L.F., 2018. Droughts over amazonia in 2005, 2010, and 2015: a cloud cover perspective. Front. Earth Sci. 6 https://doi.org/10.3389/feart.2018.00227.
Khosravi, H., Haydari, E., Shekoohizadegan, S., Zareie, S., 2017. Assessment the effect of drought on vegetation in desert area using landsat data. Egypt. J. Remote Sens. Sp. Sci. 20 https://doi.org/10.1016/j.ejrs.2016.11.007. S3–S12.
Kogan, F., Adamenko, T., Guo, W., 2013. Global and regional drought dynamics in the climate warming era. Remote Sens. Lett. 4, 364–372. https://doi.org/10.1080/2150704X.2012.736033.
Kogan, F.N., 1997. Global drought watch from space. Bull. Am. Meteorol. Soc. 78, 621–636. https://doi.org/10.1175/1520-0477(1997)078<0621:GDWFS>2.0.CO:2.
Kogan, F.N., 1995. Application of vegetation index and brightness temperature for drought detection. Adv. Sp. Res. 15, 91–100. https://doi.org/10.1016/0273-1177(95)00079-T.
Lavado, W., Espinoza, J.C., 2014. Impactos de El Niño y La Niña en las lluvias del Perú (1965-2007). Rev. Bras. Meteorol. 29, 171–182. https://doi.org/10.1590/S0102-77862014000200003.
Lin, Q., Wu, Z., Singh, V.P., Sadeghi, S.H.R., He, H., Lu, G., 2017. Correlation between hydrological drought, climatic factors, reservoir operation, and vegetation cover in the Xijiang Basin, South China. J. Hydrol. 549, 512–524. https://doi.org/10.1016/j.jhydrol.2017.04.020.
Liou, Y.A., Le, M.S., Chien, H., 2019. Normalized difference latent heat index for remote sensing of land surface energy fluxes. IEEE Trans. Geosci. Rem. Sens. 57, 1423–1433. https://doi.org/10.1109/TGRS.2018.2866555.
Madadgar, S., AghaKouchak, A., Shukla, S., Wood, A.W., Cheng, L., Hsu, K.-L., Svoboda, M., 2016. A hybrid statistical-dynamical framework for meteorological drought prediction: Application to the southwestern United States. Water Resour. Res. 52, 5095–5110. https://doi.org/10.1002/2015WR018547.
Mahto, S., Mishra, V., 2019. Does ERA-5 outperform other reanalysis productos for hydrologic applications in India? J. Geophys. Res. Atmos. https://doi.org/10.1029/2019JD031155, 0–3.
Mantua, N.J., Hare, S.R., 2002. The Pacific decadal oscillation. J. Oceanogr. 58, 35–44.
Martins, V.S., Novo, E.M.L.M., Lyapustin, A., Aragão, L.E.O.C., Freitas, S.R., Barbosa, C.C.F., 2018. Seasonal and interannual assessment of cloud cover and atmospheric constituents across the Amazon (2000–2015): insights for remote sensing and climate analysis. ISPRS J. Photogramm. Remote Sens., SI: Latin America Issue 145, 309–327. https://doi.org/10.1016/j.isprsjprs.2018.05.013.
McKee, T.B., Doesken, N.J., Kleist, J., 1993. The relation of drought frequency and duration to time scales. Proc. 8th Conf. Appl. Climatol. 17, 179–183. https://doi.org/10.1002/joc.846.
Mendoza, D.E., Samaniego, E.P., Mora, D.E., Espinoza, M.J., Campozano, L.V., 2019. Finding teleconnections from decomposed rainfall signals using dynamic harmonic regressions: a Tropical Andean case study. Clim. Dynam. 52, 4643–4670. https://doi.org/10.1007/s00382-018-4400-3.
Mishra, A.K., Singh, V.P., 2010. A review of drought concepts. J. Hydrol. 391, 202–216. https://doi.org/10.1016/j.jhydrol.2010.07.012.
Mora, D.E., Campozano, L., Cisneros, F., Wyseure, G., Willems, P., 2014. Climate changes of hydrometeorological and hydrological extremes in the Paute basin. Ecuadorean Andes. Hydrol. Earth Syst. Sci. 18, 631–648. https://doi.org/10.5194/hess-18-631-2014.
Mora, D.E., Willems, P., 2012. Decadal oscillations in rainfall and air temperature in the Paute river basin-southern andes of Ecuador. Theor. Appl. Climatol. 108, 267–282. https://doi.org/10.1007/s00704-011-0527-4.

Mortensen, E., Wu, S., Notaro, M., Vavrus, S., Montgomery, R., De Piérola, J., Sánchez, C., Block, P., 2018. Regression-based season-ahead drought prediction for southern Peru conditioned on large-scale climate variables. Hydrol. Earth Syst. Sci. 22, 287–303. https://doi.org/10.5194/hess-22-287-2018.
Mueller, B., Seneviratne, S.I., 2012. Hot days induced by precipitation deficits at the global scale. Proc. Natl. Acad. Sci. Unit. States Am. 109, 12398–12403. https://doi.org/10.1073/pnas.1204330109.
Mulualem, G.M., Liou, Y.A., 2020. Application of Artificial Neural Networks in Forecasting a Standardized Precipitation Evapotranspiration Index for the Upper Blue Nile Basin. Water, Switzerland. https://doi.org/10.3390/w12030643.
Muñoz, P., Orellana-Alvear, J., Willems, P., Célleri, R., 2018. Flash-flood forecasting in an andean mountain catchment-development of a step-wise methodology based on the random forest algorithm. Water (Switzerland) 10. https://doi.org/10.3390/w10111519.
Muradyan, V., Tepanosyan, G., Asmaryan, S., Saghatelyan, A., Dell'Acqua, F., 2019. Relationships between NDVI and climatic factors in mountain ecosystems: a case study of Armenia. Remote Sens. Appl. Soc. Environ. 14, 158–169. https://doi.org/10.1016/j.rsase.2019.03.004.
Ochoa-Tocachi, B.F., Buytaert, W., De Bievre, B., Célleri, R., Crespo, P., Villac\'\is, M., Llerena, C.A., Acosta, L., Villazón, M., Guallpa, M., others, 2016. Impacts of land use on the hydrological response of tropical Andean catchments. Hydrol. Process. 30, 4074–4089.
Oliveira-Júnior, J.F., Gois, G., Terassi, P.M., Silva Junior, C.A., Blanco, C.J.C., Sobral, B.S., Gasparini, K.A.C., 2018. Drought severity based on the SPI index and its relation to the ENSO and PDO climatic variability modes in the regions North and Northwest of the State of Rio de Janeiro - Brazil. Atmos. Res. 212, 91–105. https://doi.org/10.1016/j.atmosres.2018.04.022.
Oñate-Valdivieso, F., Uchuari, V., Oñate-Paladines, A., 2020. Large-scale climate variability patterns and drought: a case of study in south – America. Water Resour. Manag. 34, 2061–2079. https://doi.org/10.1007/s11269-020-02549-w.
Pacheco, J., Parra, N., Avilés, A., 2017. Análisis de la sequía en la cuenca del Paute mediante el índice de precipitación estandarizado (SPI). In: Azuay, U. del (Ed.), XVI Conferencia Iberoamericana de Sistemas de Información Geográfica. Cuenca - Ecuador, pp. 41–50.
Palmer, W.C., 1968. Keeping track of crop moisture conditions, nationwide: the new crop moisture index. Weatherwise 21, 156–161. https://doi.org/10.1080/00431672.1968.9932814.
Penalba, O.C., Rivera, J.A., 2016. Regional aspects of future precipitation and meteorological drought characteristics over Southern South America projected by a CMIP5 multi-model ensemble. Int. J. Climatol. 36, 974–986. https://doi.org/10.1002/joc.4398.
Piao, S., Ciais, P., Huang, Y., Shen, Z., Peng, S., Li, J., Zhou, L., Liu, H., Ma, Y., Ding, Y., Friedlingstein, P., Liu, C., Tan, K., Yu, Y., Zhang, T., Fang, J., 2010. The impacts of climate change on water resources and agriculture in China. Nature 467, 43–51. https://doi.org/10.1038/nature09364.
Quiring, S.M., Ganesh, S., 2010. Evaluating the utility of the Vegetation Condition Index (VCI) for monitoring meteorological drought in Texas. Agric. For. Meteorol. 150, 330–339. https://doi.org/10.1016/j.agrformet.2009.11.015.
Quishpe-Vásquez, C., Gámiz-Fortis, S.R., García-Valdecasas-Ojeda, M., Castro-Díez, Y., Esteban-Parra, M.J., 2019. Tropical Pacific sea surface temperature influence on seasonal streamflow variability in Ecuador. Int. J. Climatol. 1–20. https://doi.org/10.1002/joc.6047.
Rajagopalan, B., Kushnir, Y., Tourre, Y.M., 1998. Observed decadal midlatitude and tropical Atlantic climate variability are examined for their frequency the American Geophysical lb). Significant coherence. Geophys. Res. Lett. 25, 3967–3970.
Real-Rangel, R.A., Pedrozo-Acuña, A., Agustín Breña-Naranjo, J., Alcocer-Yamanaka, V.H., 2020. A drought monitoring framework for data-scarce regions. J. Hydroinf. 22, 170–185. https://doi.org/10.2166/hydro.2019.020.
Reed, R.J., Campbell, W.J., Rasmussen, L.A., Rogers, D.G., 1961. Evidence of a downward-propagating, annual wind reversal in the equatorial stratosphere. J. Geophys. Res. 66, 813–818.
Rhee, J., Im, J., Carbone, G.J., 2010. Monitoring agricultural drought for arid and humid regions using multi-sensor remote sensing data. Remote Sens. Environ. 114, 2875–2887. https://doi.org/10.1016/j.rse.2010.07.005.
Rousta, I., Olafsson, H., Moniruzzaman, M., Zhang, H., Liou, Y.A., Mushore, T.D., Gupta, A., 2020. Impacts of drought on vegetation assessed by vegetation indices and meteorological factors in Afghanistan. Rem. Sens. 12 https://doi.org/10.3390/RS12152433.
Salazar, L.F., Nobre, C.A., Oyama, M.D., 2007. Climate change consequences on the biome distribution in tropical South America. Geophys. Res. Lett. 34 https://doi.org/10.1029/2007GL029695.
Shah, R., Mishra, V., 2014. Evaluation of the reanalysis products for the monsoon season droughts in India. J. Hydrometeorol. 15, 1575–1591. https://doi.org/10.1175/JHM-D-13-0103.1.
Shahid, S., 2008. Spatial and temporal characteristics of droughts in the western part of Bangladesh. Hydrol. Process. 22, 2235–2247. https://doi.org/10.1002/hyp.6820.
Smith, C.A., Sardeshmukh, P.D., 2000. The effect of ENSO on the intraseasonal variance of surface temperatures in winter. Int. J. Climatol. 20, 1543–1557. https://doi.org/10.1002/1097-0088(20001115)20:13<1543::AID-JOC579>3.0.CO;2-A.
Şorman, A.Ü., Mehr, A.D., Hadi, S.J., 2018. Study on spatial-temporal variations of Meteorological-Agricultural droughts in Turkey. ISPRS - Int. Arch. Photogramm. Remote Sens. Spat. Inf. Sci. XLII-3/W4, 483–490. https://doi.org/10.5194/isprs-archives-XLII-3-W4-483-2018.
Stekhoven, D.J., Bühlmann, P., 2012. Missforest-Non-parametric missing value imputation for mixed-type data. Bioinformatics 28, 112–118. https://doi.org/10.1093/bioinformatics/btr597.
Sun, H., Liu, W., Wang, Y., Yuan, S., 2017. Evaluation of typical spectral vegetation indices for drought monitoring in cropland of the North China plain. IEEE J. Sel. Top. Appl. Earth Obs. Rem. Sens. 10, 5404–5411. https://doi.org/10.1109/JSTARS.2017.2734800.
Sun, H., Zhao, X., Chen, Y., Gong, A., Yang, J., 2013. A new agricultural drought monitoring index combining MODIS NDWI and day-night land surface temperatures: a case study in China. Int. J. Rem. Sens. 34, 8986–9001. https://doi.org/10.1080/01431161.2013.860659.
Sun, X., Renard, B., Thyer, M., Westra, S., Lang, M., 2015. A global analysis of the asymmetric effect of ENSO on extreme precipitation. J. Hydrol. 530, 51–65. https://doi.org/10.1016/j.jhydrol.2015.09.016.
Tadesse, T., Wilhite, D.A., Harms, S.K., Hayes, M.J., Goddard, S., 2004. Drought monitoring using data mining techniques: a case study for Nebraska, USA. Nat. Hazards 33, 137–159. https://doi.org/10.1023/B:NHAZ.0000035020.76733.0b.
Tallaksen, L.M., Van Lanen, H., 2004. Hydrological Drought: Processes and Estimation Methods for Streamflow and Groundwater. Elsevier B.V, Amsterdam, the Netherlands.
Tarek, M., Brissette, F.P., Arsenault, R., 2020. Evaluation of the ERA5 reanalysis as a potential reference dataset for hydrological modelling over North America. Hydrol. Earth Syst. Sci. 24, 2527–2544. https://doi.org/10.5194/hess-24-2527-2020.
Thomas, A.C., Reager, J.T., Famiglietti, J.S., Rodell, M., 2014. A GRACE-based water storage deficit approach for hydrological drought characterization. Geophys. Res. Lett. 41, 1537–1545. https://doi.org/10.1002/2014GL059323.
Tijdeman, E., Barker, L.J., Svoboda, M.D., Stahl, K., 2018. Natural and human influences on the link between meteorological and hydrological drought indices for a large set of catchments in the contiguous United States. Water Resour. Res. 54, 6005–6023. https://doi.org/10.1029/2017WR022412.
Tobar, V., Wyseure, G., 2018. Seasonal rainfall patterns classification, relationship to ENSO and rainfall trends in Ecuador. Int. J. Climatol. 38, 1808–1819. https://doi.org/10.1002/joc.5297.
Torrence, C., Compo, G.P., 1998. A practical Guide to wavelet analysis. Bull. Am. Meteorol. Soc. 79, 18.
Trenberth, K., 2016. The Climate Data Guide: Nino SST Indices (Nino 1+ 2, 3, 3.4, 4; ONI and TNI). Natl. Cent. Atmos. Res. Boulder, CO, USA.
Trenberth, K.E., Hurrell, J.W., 1994. Decadal atmosphere-ocean variations in the Pacific. Clim. Dynam. 9, 303–319.
Trenberth, K.E., Stepaniak, D.P., 2001. Indices of el niño evolution. J. Clim. 14, 1697–1701.
Trouet, V., Taylor, A.H., 2010. Multi-century variability in the Pacific North American circulation pattern reconstructed from tree rings. Clim. Dynam. 35, 953–963. https://doi.org/10.1007/s00382-009-0605-9.
Troup, A.J., 1965. The 'southern oscillation. Q. J. R. Meteorol. Soc. 490–506.
Tu, X., Wu, H., Singh, V.P., Chen, X., Lin, K., Xie, Y., 2018. Multivariate design of socioeconomic drought and impact of water reservoirs. J. Hydrol. 566, 192–204.
UNESCO, U.-W., 2020. United Nations World Water Development Report 2020: Water and Climate Change. UNESCO, Paris, France.

Valverde-Arias, O., Garrido, A., Valencia, J.L., Tarquis, A.M., 2018. Using geographical information system to generate a drought risk map for rice cultivation: case study in Babahoyo canton (Ecuador). Biosyst. Eng. 168, 26–41. https://doi.org/10.1016/j.biosystemseng.2017.08.007.

Van Loon, A.F., 2015. Hydrological Drought Explained, 2. Wiley Interdiscip. Rev. Water, pp. 359–392. https://doi.org/10.1002/wat2.1085.

Van Loon, A.F., Gleeson, T., Clark, J., Van Dijk, A.I.J.M., Stahl, K., Hannaford, J., Di Baldassarre, G., Teuling, A.J., Tallaksen, L.M., Uijlenhoet, R., Hannah, D.M., Sheffield, J., Svoboda, M., Verbeiren, B., Wagener, T., Rangecroft, S., Wanders, N., Van Lanen, H.A.J., 2016a. Drought in the anthropocene. Nat. Geosci. 9, 89–91. https://doi.org/10.1038/ngeo2646.

Van Loon, A.F., Laaha, G., 2015. Hydrological drought severity explained by climate and catchment characteristics. J. Hydrol. 526, 3–14. https://doi.org/10.1016/j.jhydrol.2014.10.059.

Van Loon, A.F., Stahl, K., Di Baldassarre, G., Clark, J., Rangecroft, S., Wanders, N., Gleeson, T., Van Dijk, A.I.J.M., Tallaksen, L.M., Hannaford, J., Uijlenhoet, R., Teuling, A.J., Hannah, D.M., Sheffield, J., Svoboda, M., Verbeiren, B., Wagener, T., Van Lanen, H.A.J., 2016b. Drought in a human-modified world: reframing drought definitions, understanding, and analysis approaches. Hydrol. Earth Syst. Sci. 20, 3631–3650. https://doi.org/10.5194/hess-20-3631-2016.

Vicente-Serrano, S.M., 2007. Evaluating the impact of drought using remote sensing in a mediterranean, semi-arid region. Nat. Hazards 40, 173–208. https://doi.org/10.1007/s11069-006-0009-7.

Vicente-Serrano, S.M., Aguilar, E., Martínez, R., Martín-Hernández, N., Azorin-Molina, C., Sanchez-Lorenzo, A., El Kenawy, A., Tomás-Burguera, M., Moran-Tejeda, E., López-Moreno, J.I., Revuelto, J., Beguería, S., Nieto, J.J., Drumond, A., Gimeno, L., Nieto, R., 2017. The complex influence of ENSO on droughts in Ecuador. Clim. Dynam. 48, 405–427. https://doi.org/10.1007/s00382-016-3082-y.

Vicente-Serrano, S.M., López-Moreno, J.I., Beguería, S., Lorenzo-Lacruz, J., Azorin-Molina, C., Morán-Tejeda, E., 2012. Accurate computation of a streamflow drought index. J. Hydrol. Eng. 17, 318–332. https://doi.org/10.1061/(ASCE)HE.1943-5584.0000433.

Vicente-Serrano, S.M., López-Moreno, J.I., Lorenzo-Lacruz, J., El Kenawy, A., Azorín-Molina, C., Morán-Tejeda, E., Pasho, E., Zabalza, J., Beguería, S., Angulo-Martínez, M., 2011. The NAO impact on droughts in the Mediterranean region. Hydrol. Socioecon. Ecol. Impacts North Atl. Oscil. Mediterr. Reg. 46, 23–40. https://doi.org/10.1007/978-94-007-1372-7.

Vuille, M., Bradley, R., Keimig, F., 2000. Climate variability in the andes of Ecuador and its relation to tropical Pacific and Atlantic sea surface temperature anomalies. J. Clim. 13, 2520–2535.

Wang, F., Lai, H., Li, Y., Feng, K., Zhang, Z., Tian, Q., Zhu, X., Yang, H., 2022. Dynamic variation of meteorological drought and its relationships with agricultural drought across China. Agric. Water Manag. 261, 107301 https://doi.org/10.1016/j.agwat.2021.107301.

Wang, H., Chen, Y., Pan, Y., Chen, Z., Ren, Z., 2019. Assessment of candidate distributions for SPI/SPEI and sensitivity of drought to climatic variables in China. Int. J. Climatol. https://doi.org/10.1002/joc.6081.

Wang, M., Jiang, S., Ren, L., Xu, C.Y., Yuan, F., Liu, Y., Yang, X., 2020. An approach for identification and quantification of hydrological drought termination characteristics of natural and human-influenced series. J. Hydrol. 590 https://doi.org/10.1016/j.jhydrol.2020.125384.

Wang, W., Ertsen, M.W., Svoboda, M.D., Hafeez, M., 2016. Propagation of drought: from meteorological drought to agricultural and hydrological drought. Adv. Meteorol. https://doi.org/10.1155/2016/6547209, 2016.

Wardlow, B.D., Anderson, M.C., Verdin, J.P., 2012. Remote Sensing of Drought: Innovative Monitoring Approaches. CRC Press.

Wilhite, D., 2000. Drought: a Global Assessment. Routledge.

Wilhite, D.A., Glantz, M.H., 1985. Understanding : the drought phenomenon : the role of definitions. Water Int. 10, 111–120. https://doi.org/10.1080/02508068508686328.

Wolter, K., Timlin, M.S., 2011. El Niño/Southern Oscillation behaviour since 1871 as diagnosed in an extended multivariate ENSO index (MEI.ext). Int. J. Climatol. 31, 1074–1087. https://doi.org/10.1002/joc.2336.

Wu, J., Chen, X., Gao, L., Yao, H., Chen, Y., Liu, M., 2016. Response of hydrological drought to meteorological drought under the influence of large reservoir. Adv. Meteorol. 2016.

Wu, J., Chen, X., Yao, H., Gao, L., Chen, Y., Liu, M., 2017. Non-linear relationship of hydrological drought responding to meteorological drought and impact of a large reservoir. J. Hydrol. 551, 495–507. https://doi.org/10.1016/j.jhydrol.2017.06.029.

Yu, J.Y., Kao, H.Y., Lee, T., Kim, S.T., 2011. Subsurface ocean temperature indices for central-Pacific and Eastern-Pacific types of El Niño and La Niña events. Theor. Appl. Climatol. 103, 337–344. https://doi.org/10.1007/s00704-010-0307-6.

Yu, M., Liu, X., Li, Q., 2020. Responses of meteorological drought-hydrological drought propagation to watershed scales in the upper Huaihe River basin, China. Environ. Sci. Pollut. Res. 27, 17561–17570. https://doi.org/10.1007/s11356-019-06413-2.

Zambrano, F., Lillo-Saavedra, M., Verbist, K., Lagos, O., 2016. Sixteen years of agricultural drought assessment of the BioBío region in Chile using a 250 m resolution vegetation condition index (VCI). Rem. Sens. 8, 530. https://doi.org/10.3390/rs8060530.

Zambrano Mera, Y.E., Rivadeneira Vera, J.F., Pérez-Martín, M.Á., 2018. Linking El Niño Southern Oscillation for early drought detection in tropical climates: the Ecuadorian coast. Sci. Total Environ. 643, 193–207. https://doi.org/10.1016/j.scitotenv.2018.06.160.

Zhang, Y., You, Q., Lin, H., Chen, C., 2015. Analysis of dry/wet conditions in the Gan River Basin, China, and their association with large-scale atmospheric circulation. Global Planet. Change 133, 309–317. https://doi.org/10.1016/j.gloplacha.2015.09.005.

Zhiña, D., Montenegro, M., Montalván, L., Mendoza, D., Contreras, J., Campozano, L., Avilés, A., 2019. Climate change influences of temporal and spatial drought variation in the andean high mountain basin. Atmosphere 10, 558. https://doi.org/10.3390/atmos10090558.

Zhong, S., Sun, Z., Di, L., 2021. Characteristics of vegetation response to drought in the CONUS based on long-term remote sensing and meteorological data. Ecol. Indicat. 127, 107767 https://doi.org/10.1016/j.ecolind.2021.107767.

Zou, L., Cao, S., Sanchez-Azofeifa, A., 2020. Evaluating the utility of various drought indices to monitor meteorological drought in Tropical Dry Forests. Int. J. Biometeorol. 64, 701–711. https://doi.org/10.1007/s00484-019-01858-z.